



Study of the Physical Properties of *Pinus Halepensis* of Oran Application to the Flammability

H.Boutchiche¹, F. Z. Sabi¹, O. Mosbah¹, A. Sahila¹, S.M. Terrah¹, N. Zekri^{1*}

¹**Université des Sciences et de la Technologie d'Oran, LEPM BP 1505 El Mnaouer Oran, Algeria,*

**Corresponding Author. {[nzeكري@yahoo.com](mailto:nzekri@yahoo.com)} <https://orcid.org/0000-0001-7325-4114>*

Received. October 01, 2019. Accepted. November 21, 2019. Published. March 19, 2020.

DOI: <https://doi.org/10.58681/ajrt.20040106>

Abstract. Physical parameters (density, packing ratio etc.) of *pinus halepensis* needles harvested from the campus of Université des Sciences et de la Technologie d'Oran are measured and used in a simple physical model for ignition. The numerical results obtained by the model are compared with ignition time measurements for the same fuel using a cone calorimeter. The ignition time seems over-estimated by the model. Further discussions on the reasons of this discrepancy are provided.

Keywords. Physical parameters, Flammability, *Pinus halepensis*, Ignition time.

INTRODUCTION

Every year fires rip across the earth with alarming ferocity and deadly consequences (Martin 2016). They are a real threat to both people and the ecosystem. Despite technological and scientific development, fire initiation and propagation remain complex and unpredictable.

Different models are used in the study of forest fires behavior. They are classically grouped into statistical, empirical, and physical models (Weber 1991). Since the fuel is randomly organized in wildlands, Statistical modeling seems to be the most appropriate for predicting forest fires.

Numerical codes like FARSITE (Finney 1998, Finney 2004) and BEHAVE (Andrews 1989) were developed to simulate fire spread for homogeneous fuels, but they often failed to reproduce fire patterns and contours in wildlands because of the heterogeneity caused by different types of vegetation, heterogeneous topography and meteorological instability.

The Small World Network model has been initially proposed in 2005 (Zekri et al. 2005) to predict fire spread in heterogeneous systems. Physical parameters, like radiation effects of the flames and thermal behavior of the fuel, were successfully introduced in this model to validate with better accuracy both historical fire of Lançon in southern France in 2005, and the experimental fires of Savane in 1992 (Porterie et al.2008, Adou et al. 2011). However, experimental laboratory fire spread results obtained recently in Portugal (Viegas and Zekri 2015) were overestimated by the model. The ignition part of the model uses conservation

energy of the fuel (Koo et al. 2005), which requires the knowledge of physical parameters like the fuel density, the specific heat and the packing ratio. The parameters used in the model were always taken from literature. However, the strengths of these parameters can change for the same vegetation from a region to another or from a tree to another or even from a season to another for the same tree (Jervis and Rain 2016), which influence significantly the ignition time.

In this work, the density, surface to volume ratio and the packing ratio of *pinus halepensis* needles harvested at the campus of USTO University are measured. The needles are ignited using a cone calorimeter, and the ignition time is determined. The measured parameters are included in the energy conservation model (Koo et al. 2005) to compare the simulated ignition time with the experimental results.

MODEL DESCRIPTION

Let us consider the experimental conditions (see § 3), where a fuel sample is ignited by a cone calorimeter. The present model assumes that the sample receives a constant radiative heat flux q''_{inc} (expressed in kW/m²) from the cone calorimeter (the induced convective flux is neglected). The effective heat flux q''_{eff} absorbed by the sample is:

$$q''_{eff} = q''_{inc} - q''_{lost} \quad (1)$$

The heat flux lost from the sample q''_{lost} depends on its temperature increase. It is composed of a radiative and a convective part (the conductive heat transfer is neglected):

$$q''_{lost} = h_c(T - T_0) + \sigma \varepsilon_{fb}(T^4 - T_0^4) \quad (2)$$

Where h_c is the convection heat transfer coefficient, ε_{fb} the fuel emissivity, σ the Stephen-Boltzmann constant and $T_0 = 300 K$ the ambient temperature. If the sample temperature is close to the ambient temperature ($T \rightarrow T_0$), equation (2) is linearized, and the lost heat flux is reduced to an effective convective flux (see equation 7.24 of (Quintiere 2006)). For high temperatures (i.e. near the ignition temperature) the nonlinear part of (2) is dominant, and the heat flux is mainly lost by radiations. The energy accumulated by the sample during its ignition period allows the surface temperature to reach ignition temperature. This latter is reached in three steps: *i*) the increase of the moist sample temperature up to boiling (373 K), *ii*) the evaporation of water mass m_w of the moist sample, *iii*) the increase of the dry sample temperature (pyrolysis) until it reaches the ignition temperature (here $T_{ign} = 560K$). Neglecting the heat of water desorption and heat of conduction, the energy conservation for a solid fuel of surface S in the thermally thin approximation (Quintiere 2006, Torero 2016) is:

$$\int_0^{t_{ign}} q''_{eff} S dt = \begin{cases} \int_{T_0}^{373 K} (m_{dry}c_p^f + m_w c_p^w) dT + \\ \int_{m_w}^0 L_v(373 K) dm_w + \\ \int_{373 K}^{T_{ign}} m_{dry} c_p^f dT \end{cases} \quad (3)$$

Here, S is the surface of the solid fuel (in m²), $c_p^f = 1827 J.kg^{-1}.K^{-1}$ (Lamorlette et al. 2015) and $c_p^w = 4182 J.kg^{-1}.K^{-1}$ (Wagner and Kretschmar 2010) are the specific heat of the dry fuel and water content respectively, $L_v = 2257 kJ/kg$ is the latent heat of water at 373 K, and (m_{dry}/m_w) are the dry fuel/water masses exposed to the incident heat flux q''_{inc} delivered by the cone calorimeter.

As the fuel considered here is porous (Fig.1), its effective surface is different from that of the sample holder. It is necessary to introduce in (3) the packing ratio ϕ , that is the ratio of the volume of the solid part (particles) to the total volume of the fuel bed for the same mass. In the case of a completely dry fuel, its mass m is related to the packing ratio as:

$$m = \phi . \rho . S . d \quad (4)$$

Where ρ is the fuel density, d the sample thickness and S is the surface of the sample holder, the effective surface is thus $S_{eff} = \phi S$ ($\phi \leq 1$). In the case of a moist fuel, it is composed of a dry (m_{dry}) and water (m_w) part ($m = m_{dry} + m_w$). The moisture content is defined on a dry basis as:

$$h_d = m_w / m_{dry} \quad (5)$$

On wet basis we have:

$$h_w = \frac{m_w}{m_{dry} + m_w} \quad (6)$$

using (5) equation 4 becomes:

$$m = m_{dry}(1 + h_d) = \phi(h_d) \cdot \rho(h_d) \cdot S \cdot d \quad (7)$$



Fig. 1. A view of *Pinus halepensis* needles in the sample holder of 10cm diameter and 5cm height.

The packing ratio is determined from the measurements of the mass, the density and the moisture content on the dry basis. Introducing (7) in (3) the conservation energy for the porous fuel becomes:

$$\int_0^{t_{ign}} q''_{eff} S dt = \begin{cases} \int_{T_0}^{373 K} [\phi(h_d) \cdot \rho(h_d) \cdot S \cdot d \cdot c_p^f + h_d \phi(h_d) \cdot \rho(h_d) \cdot S \cdot d \cdot c_p^w] \frac{dT}{1+h_d} + \\ \int_{m_w}^0 \phi(h_d) \cdot \rho(h_d) \cdot L_v(373 K) \cdot S \cdot \frac{dh_d}{1+h_d} + \\ \int_{373 K}^{T_{ign}} \phi(h_d) \cdot \rho(h_d) \cdot S \cdot d \cdot c_p^f \frac{dT}{1+h_d} \end{cases} \quad (8)$$

Note here the difference with the energy conservation presented by Koo et al., where the packing ratio was estimated from the dry basis. It is expected from the theory of ignition (Quintiere 2006) that the inverse ignition time behaves linearly with the incident heat flux. For a solid thin material of thickness d , density ρ and specific heat c_p we have:

$$\frac{1}{t_{ign}} \approx C \cdot q''_{inc} \quad \text{with} \quad C = \left(\rho \cdot d \cdot c_p \cdot (T_{ign} - T_0) \right)^{-1} \quad (9)$$

However, this behavior is valid only in the limit of large fluxes where the ignition time is small (the density and specific heat are assumed to be constant). It does not apply for small incident heat fluxes, particularly near the critical heat fluxes. In order to model both high and low fluxes, equation 8 is solved here numerically by using the second order Runge-Kutta method to obtain the ignition time dependence on the incident heat flux.

EXPERIMENTAL SETUP

Physical parameters measurement

For the modeling of the flammability of *pinus halepensis* (*Ph*), the following physical parameters are required for needles: the density ρ , the Surface to Volume Ratio *SVR* (for the calculation of the rate of spread), and the packing ratio ϕ for the porous sample. The remaining parameters (the specific heat C_p and latent heat L_v) are deduced from literature at 300K. The density measurement involves the determination of the mass and the volume of a single needle. The *SVR* requires the volume and surface of the needle. The packing ratio estimation requires also the mass and thickness of the whole sample to be burned. As the flammability measurements are realized both for fresh needles (during the day of harvest) and dry ones (dried using a microwave oven at 800W during 3mn), the parameters (ρ and *SVR*) are measured for dry and fresh samples.

Determination of the density and SVR of the needles

The density of *Ph* needles is defined as:

$$\rho = \frac{m}{V} \quad (10)$$

The mass m is weighted using a balance (Kern PCB 350) with an accuracy of 1mg, and the volume V is estimated by two different methods: the metric and the pycnometer method.

The metric method

The needle section of *Ph* is assimilated to a half-ellipse. The smaller axis corresponds to its thickness e and the larger one to its diameter D (Bartoli 2016). These lengths were measured using a digital caliper with an accuracy of $10^{-5} m$. The measurement is repeated for 100 needles (for each needle three positions were considered), and the average quantity is determined.



Fig.2. A schematic figure of *Pinus halepensis* needle.

The volume is thus calculated from these average quantities as:

$$V = \pi \frac{D}{4} e L \quad (11)$$

For the present measurements, the average length of dry and fresh needles is $L \cong 50mm$. The other average dimensions are $e = 0.51mm$ and $D = 0.69mm$ for dry needles, and $e = 0,52mm$ and $D = 0.79mm$ for fresh needles.

Pycnometer method

In this method, the needles volume is determined in two steps. The first step consists in weighting both the pycnometer completely filled with water (Fig. 3) and 8 *Ph* needles. In the second step, the needles are introduced in the pycnometer which is weighted after rapidly removing the lost water. The lost water mass (m_{lost}) is the difference of the weights determined in the two steps. The volume of the needles is thus obtained using the density of the distilled water ($\rho_{water} = 998.21 \frac{kg}{m^3}$ at 20°C see Wagner and Kretzschmar 2010). The volume of lost water V_{lost} is thus deduced from the mass m_{lost} by $V_{lost} = m_{lost} / \rho_{water}$.

In order to avoid rehydration of the sample it is necessary to make the measurements within the minimum possible time.

The surface to volume ratio *SVR* of the needle is also determined from these quantities by the metric method as (see Bartoli 2016):

$$SVR = \frac{4(D+P)}{\pi D e} \quad (12)$$

Where the half-ellipse perimeter P is given by

$$P = \pi \sqrt{\frac{e^2 + \frac{D^2}{4}}{2}} \quad (13)$$



Fig. 3. The pycnometer used in measurement.

The following table shows the average values of ρ and SVR obtained using the methods described above.

Table 1. Comparison of measured parameters with literature using the metric and pycnometer.

pH	Method	ρ_{avg} (kg/m ³)	SVR^* (m ⁻¹)
Dry	Metric	716 ± 96	7440 ± 360
	Pycnometer	680 ± 33	
Fresh	Literature	789 (Lamorlette et al. 2015)	7377 (Lamorlette et al. 2015)
	Metric	1219 ± 98	6940 ± 330
	Pycnometer	1087 ± 3	

(* the pycnometer measures only the volume)

Determination of the packing ratio

The determination of the packing ratio ϕ from (7) requires also the mass and dimensions of the sample to be submitted to the cone calorimeter (Fig.1). Here the sample mass is $m=10$ g and its thickness is $d= 1.2$ cm and the sample surface is $S= 7.85 \cdot 10^{-3} m^2$, The packing ratio obtained is: $\phi(h_d) = 0.148$, with the moisture content $h_w = 52\%$ ($h_d = 1.08$). Regarding the dry sample, it is compacted so that the thickness remains constant (1.2 cm). It is important to notice from (4), (5) and (7) the following relation between dry and moist samples:

$$\phi(h_d)\rho(h_d) = (1 + h_d) \cdot \phi(0)\rho(0) \quad (14)$$

Replacing (14) in (8), allows to use only the density and packing ratio of dry samples. Equation 8 becomes:

$$\int_0^{t_{ign}} q''_{eff} dt = \begin{cases} \int_{T_0}^{373 K} \phi(0) \cdot \rho(0) \cdot d \cdot [c_p^f + h_d c_p^w] dT + \\ \int_{m_w}^0 \phi(0) \cdot \rho(0) \cdot d \cdot L_v(373 K) \cdot dh_d + \\ \int_{373 K}^{T_{ign}} \phi(0) \cdot \rho(0) \cdot d \cdot c_p^f dT \end{cases} \quad (15)$$

Flammability measurement

A cone calorimeter with an electrical resistance of 5000 W power, used as a heat source, provides a radiation heat flux to the fuel sample. The vegetation samples described above were placed in a cylindrical holder of 10 cm diameter of a mesh shape. For fresh samples 10g of *Ph* needles (corresponding to load of about 1.27 kg/m²) are burned. For dried samples, the whole dried needles obtained from 10g fresh *Ph* needles are burned (i.e., 10/(1 + h_d)g). The cone is schematically shown in the inset of figure 4.

The sample is placed at different distances from the heat source, so that it receives radiation heat fluxes of magnitudes ranging from 9 to 25 kW/m² (see the calibration in Fig. 4). The incident heat flux at the top surface position of the sample is calibrated by using a water-cooled heat flux sensor of type Hukseflux SBG 01 working in the range 0-200kW/m². The ignition process is controlled by a pilot flame located 1 cm above the sample top surface according to ASTM 1354 standards (ASTM 2017), and the ignition time is recorded. The fuel moisture content can be defined on dry or wet basis.

Fresh *Ph* needles harvested from the campus of USTO University are at about 52% moisture. The harvest and ignition are realized within the same day in August 2019. The ignition time t_{ign} is recorded if the flame persistence time is greater than 4s. If smoldering combustion is observed with a complete oxidation of the fuel in its solid phase it is considered that flaming ignition cannot occur (Rein 2016). The exposition time to the heat flux varies from a test to another, and can take up to 75 minutes.

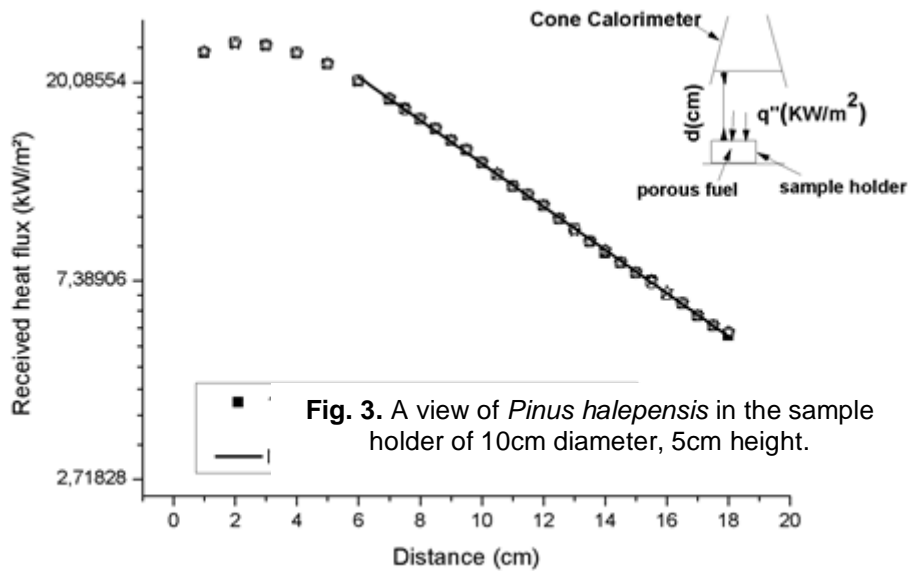


Fig. 4. A schematic representation of the calibration flux and the experimental setup.

Due to the heterogeneity of the sample structure, up to three (3) ignition tests were realized for each heat flux. The average ignition time $\langle t_{ign} \rangle$ is the mean of the three recorded tests. The tests were conducted in a draft-free room with temperature and relative humidity in the ranges of 23-25°C and 50-72%.

RESULTS AND DISCUSSION

48

In this section, the behavior of numerical simulation of $1/\langle t_{ign} \rangle$ is compared to that of experimental results by varying the incident heat flux. Ignition theory predicts a linear dependence on the incident flux (see equation 9). The slope depends on the density, temperature difference between ambient and ignition, and the specific heat.

In figure 5, the comparison concerns dry (Fig.5a) and fresh (Fig.5b) *Ph* needles. The ignition time results for fresh fuel are one magnitude larger than those of dry fuel. The linear behavior predicted by ignition theory (9) is observed for all fluxes larger than 5 kW/m^2 in simulation results (below this flux strength a transition to non-ignition is expected, see Sabi et al. 2018). The physical parameters used here (see section 2 and table 1) yield $C \approx 0.24 \times 10^{-3} \text{ m}^2/\text{kJ}$, which is much smaller than the slopes of simulation results for both fresh and dry fuels. In fact ignition theory is predicted for solid fuels, while the simulations (8) concern porous fuels (needles). The fuel density is replaced by $\rho \cdot \phi$, and from (4, 5) the constant C in (9) becomes:

$$C = \left(\frac{m}{s} (c_p^f + h_d c_p^w) (T_{ign} - T_0) \right)^{-1} \quad (16)$$

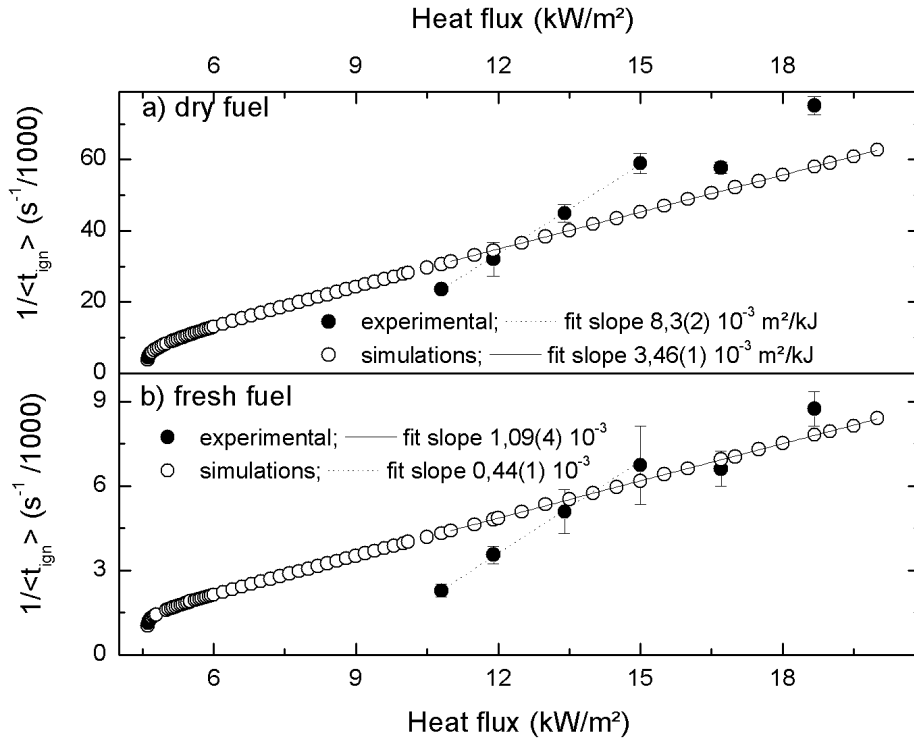


Fig.5. The average inverse ignition time vs. incident heat flux for a) dry *Ph*, b) fresh *Ph* needles.

The packing ratio of the dried fuel obtained from 10g fresh fuel ($m = 4.8\text{g}$, $h_d = 0$) is $\phi \sim 0.071$, which yields a constant C around $3.44 \times 10^{-3} \text{ m}^2/\text{kJ}$. This value is in good agreement with the slope of simulation results in figure 5a within the statistical errors. The same agreement is obtained with the slope of simulation results in figure 5b for fresh needles with $m = 10\text{g}$ and $h_d = 108.3\%$, where from (16) the constant C is 0.48×10^{-3} .

The linear behavior discussed above is restricted to fluxes in the range $10\text{--}15\text{ kW/m}^2$ for experimental data (both for fresh and dry fuels) with a much higher slope than that of simulation results. For larger fluxes, the ignition time seems to fluctuate. These fluctuations may be due to the incident flux attenuation by a large amount of organic components emitted by the fuel. The smoke formed by these components is enhanced as the flux increases. The

attenuation is enhanced for fresh samples (Fig.5b), where even the data at 15kW/m² is also affected (the linear fit is much better for dry samples).

The under-estimation by simulations of the slope for experimental data at high fluxes may be due to the physical parameters (specific heat, fuel density and packing ratio) which are taken as constant in the simulation model. In fact, as the fuel temperature increases during its exposition to the heat flux (of the cone calorimeter), its structure changes significantly leading to the increase of the specific heat and decrease of the mass (by the emission of organic components and water for fresh fuels). Hence, a competition effect on the ignition time occurs between these two parameters. Indeed, an increase of c_p^f leads to a decrease of the slope in figure 5, whereas the decrease of the fuel mass leads to the increase of the slope. As the slope of the experimental data is larger, the effect of the mass loss dominates. The ratio of simulation to experimental slopes is slightly smaller for fresh fuels (0.408) than dry ones (0.423), unlike the dominant trend of mass losses (see the above discussion). This contradictory result may be due to the gas/air mixture lower flammability limit which is not accounted in simulations.

Therefore, the difference between experimental data and simulation results is probably due to some temperature behaviors of the physical parameters not accounted for in simulation model. Let us cite the most important of them:

- The fuel mass decreases with temperature.
- The specific heat increases with temperature.
- Desorption of water,
- Water evaporation occurs at different temperatures, and is accompanied by organic components emission (Ciccioli et al. 2014) instead of evaporation only at 373K.
- The incident heat flux is attenuated by water and volatiles emission.
- Ignition process occurs when the flammable gas/air mixture reaches the lower flammability limit.

CONCLUSIONS

Physical parameters of *pinus halepensis* needles were measured and included in a simple physical model to study their flammability properties. Simulation results reproduce the linear trend predicted by ignition theory. However, they cannot reproduce the experimental data.

The most important phenomena that induce the discrepancy with experimental data are physical changes and chemical reactions that occur at the surface of the solid fuel during heating, and the gas mixture diffusion. Furthermore, the model uses a constant mass of the sample and specific heat. However, these parameters change with temperature. A competition effect occurs between the increase of the specific heat and the decrease of the mass. To overcome this problem, a measure of the specific heat and mass loss as a function of temperature should be included in simulation model. This is the subject of a forthcoming work.

REFERENCES

- ASTM International, Designation E 1354-17, 2017. Standard Test Method for Heat and Visible Smoke Release Rates for Materials and Products Using an Oxygen Consumption Calorimeter. ASTM International, West Conshohocken, PA.
- Adou, J. K., Billaud, Y., Brou, D. A., Clerc, J. P., Consalvi, J. L., Fuentes, A., Kaiss, A., Nmira, F., Porterie, B., Zekri, L., & Zekri, N. (2010). Simulating wildfire patterns using a small-world network model. *Ecological Modelling*, 221(11). <https://doi.org/10.1016/j.ecolmodel.2010.02.015>

- Andrews, P. P. P. L. (1986). BEHAVE : Fire behavior prediction and fuel modeling system - BURN subsystem, part 1. *USDA Forest Service, Intermountain Forest and Range Experiment Station, General Technical Report, INT-194*.
- Bartoli, P., 2016. Feux de forêt : amélioration de la connaissance du couplage combustible-flamme, Université de Corse-Pascal Paoli, Université d' Edinburgh. Phd thesis.
- Ciccioli, P., Centritto, M., & Loreto, F. (2014). Biogenic volatile organic compound emissions from vegetation fires. In *Plant, Cell and Environment* (Vol. 37, Issue 8). <https://doi.org/10.1111/pce.12336>
- Finney, M. A. (1998). FARSITE: Fire Area Simulator - Model Development and Evaluation. *USDA Forest Service - Research Papers RMRS, RMRS-RP-4*.
- Jervis, F. X., & Rein, G. (2016). Experimental study on the burning behaviour of *Pinus halepensis* needles using small-scale fire calorimetry of live, aged and dead samples. *Fire and Materials*, 40(3). <https://doi.org/10.1002/fam.2293>
- Koo, E., Pagni, P., Woycheese, J., Stephens, S., Weise, D., & Huff, J. (2005). A simple physical model for forest fire spread rate. *Fire Safety Science*. <https://doi.org/10.3801/IAFSS.FSS.8-851>
- Lamorlette, A., el Houssami, M., Thomas, J. C., Simeoni, A., & Morvan, D. (2015). A dimensional analysis of forest fuel layer ignition model: Application to the ignition of pine needle litters. *Journal of Fire Sciences*, 33(4). <https://doi.org/10.1177/0734904115591177>
- Martin, D., Tomida, M., & Meacham, B. (2016). Environmental impact of fire. *Fire Science Reviews*, 5, 1-21. <https://doi.org/10.1186/s40038-016-0014-1>
- Rein, G., 2016, Smoldering combustion, in: M.J.Hurley (Ed), *SFPE Handbook of fire protection engineering*, chap.19, Springer, Heidelberg, 581-603.
- Porterie, B., Kaiss, A., Clerc, J. P., Zekri, L., & Zekri, N. (2008). Universal scaling in wildfire fractal propagation. *Applied Physics Letters*, 93(20). <https://doi.org/10.1063/1.3030980>
- Quintiere, J. G. (2006). Fundamentals of Fire Phenomena. In *Fundamentals of Fire Phenomena*. <https://doi.org/10.1002/0470091150>
- Sabi, F. Z., & et. al. (2018). Ignition/non ignition phase transition. In *Advances in forest fire research 2018*. https://doi.org/10.14195/978-989-26-16-506_55
- Torero, J. (2016). Flaming ignition of solid fuels. In *SFPE Handbook of Fire Protection Engineering, Fifth Edition*. https://doi.org/10.1007/978-1-4939-2565-0_21
- Viegas, D.X., and Zekri, N., 2015. Measurement of the rate of spread of shrub in laboratory scale. Private Communication
- Wagner, W., Kretschmar, H.J., 2010. Properties of Water and Steam, in: VDI-GVC (Ed), *VDI Heat Atlas*, Springer-Verlag, Berlin Heidelberg 2nd ed, p.154.
- Weber, R. O. (1991). Modelling fire spread through fuel beds. In *Progress in Energy and Combustion Science* (Vol. 17, Issue 1). [https://doi.org/10.1016/0360-1285\(91\)90003-6](https://doi.org/10.1016/0360-1285(91)90003-6)
- Zekri, N., Porterie, B., Clerc, J. P., & Loraud, J. C. (2005). Propagation in a two-dimensional weighted local small-world network. *Physical Review E - Statistical, Nonlinear, and Soft Matter Physics*, 71(4). <https://doi.org/10.1103/PhysRevE.71.046121>